Study of the Photon Propagation Paradox

by

Amy West, B.S.

A Thesis

In

Applied of Physics

Submitted to the Graduate Faculty

Of Texas Tech University

Partial Fulfillment of

The Requirement for

the Degree of

MASTER OF SCIENCE

Approved

Dr. Luis Grave de Peralta
Chair of Committee

Dr. Ayrton Bernussi

Peggy Gordon Miller

Dean of the Graduate School

May, 2012

TABLE OF CONTENTS

ABSTRACT

Surface Plasmon Polaritions(SPP) are electromagnetic waves that travel in the interface of a metal and dielectric and are coupled to collective oscillation of free electrons. SPP tomography is an imaging technique that permits the study of the interference features formed at the metal-air interface of a sample due to the superposition of SPP beams, with high fidelity.

We present an experimental study on the formation of SPP standing waves. We demonstrate that SPP tomography in a quantum eraser arrangement permits the detection of photons passing through the dark fringes of the observed interference pattern. We present a comprehensive explanation of how photons could pass undetected across the regions occupied by the dark fringes.

LIST OF FIGURES

CHAPTER I

INTRODUCTION

Surface Plasmom Polaritons(SPP) are electromagnetic waves that travel in the interface of a metal and dielectric and is coupled to collective oscillation of free electrons[1]. The quasi two-dimensional (2D) nature of SPPs has motivated fundamental studies in 2D light propagation, interference, and diffraction phenomena which are needed for design and simulation of SPP-based devices. SPPs are the result of the interaction between longitudinal charge-density and quasi-two-dimensional electromagnetic waves that are confined to the interface between a conductor and a dielectric material each with permittivity ε_m and ε_d respectively. One of the most commonly used methods to excite SPPs is the Kretschmann-Raether Configuration [2]. This method utilizes evanescent waves in a thin metal film that is deposited over a prism to couple and excite SPPs. Figure 1.1 illustrates the Kretschmann-Raether Configuration.

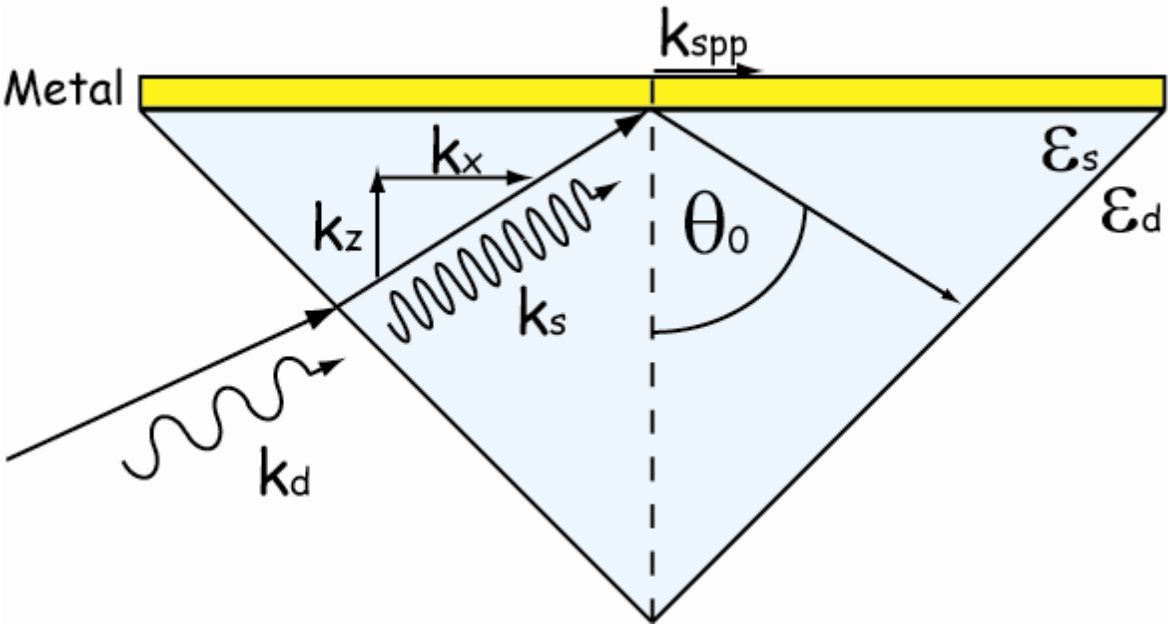

Fig.1.1 An illustration of the Kretschmann-Raether geometry used to excite a SPPs [3].

In this geometry, a thin layer of metal (such as gold) is placed in contact with a prism. Light is incident through the prism. At the ideal angle of incidence, θ_{SPP}, the energy and momentum of the light is transferred into the surface plasmons. θ_{SPP} is found by finding the angle that satisfies the matched wavevector condition:

$$k_x = \frac{2\pi}{\lambda}\sqrt{\epsilon_s}\sin\theta_{SPP} \quad (1.1)$$

Where ε_s is the permittivity of the substrate and λ is the wavelength of the light in the vacuum. When θ_{SPP} satisfies this condition, we find that the reflectivity of the light drops dramatically as the light is absorbed and coupled into SPPs. The relationship between the incident and the reflectivity of the light is shown in figure 1.2.

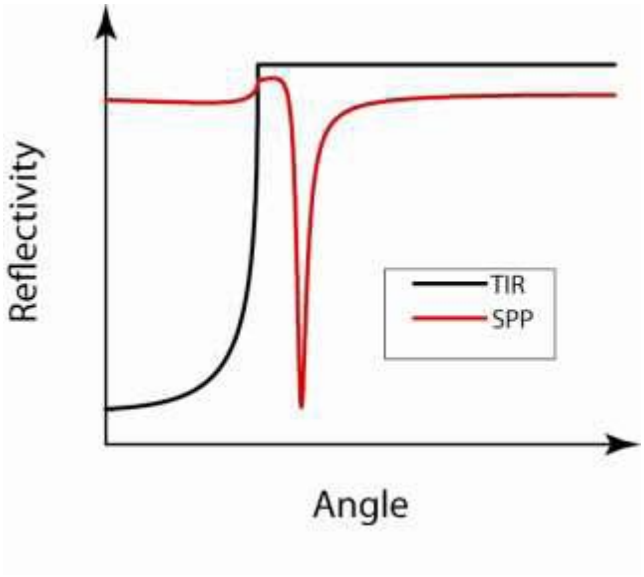

Figure 1.2 Graph of reflectivity versus angle for a glass/air and glass/metal/air structures[3].

As the incidence angle is increased, there is a rise in the reflectivity at approximately the same position as seen if there were no metal layer on the prism. Total internal reflection, TIR, occurs at the same location regardless of the existence of the metal on the prism. Shortly after this angle, a sharp dip occurs signifying the absorption maximum as the SPP coupling conditions are met. The SPPs propagates on the interface but some of the light will penetrate into the metal and be lost. Because of this loss, we can find that the intensity of the SPP goes as:

$$I(x) = I_o e^{-\frac{x}{L}} \quad (1.2)$$

Where L is the propagation length of the SPP.

SPPs can also be excited by generating light in close proximity to the metal surface so that some of the light couples evanescently to the interface [2]. In our case, this effect was achieved by depositing dielectric ridges on the metal surface, thereby creating an SPP waveguide. This is knows as a Dielectric Loaded Surface Plasmon Polariton Waveguide, or DLSSPWs [4]. The light that leaks from the waveguide through the sample is called leakage radiation. The leaked light was collected by the arrangement as shown in figure 1.3.

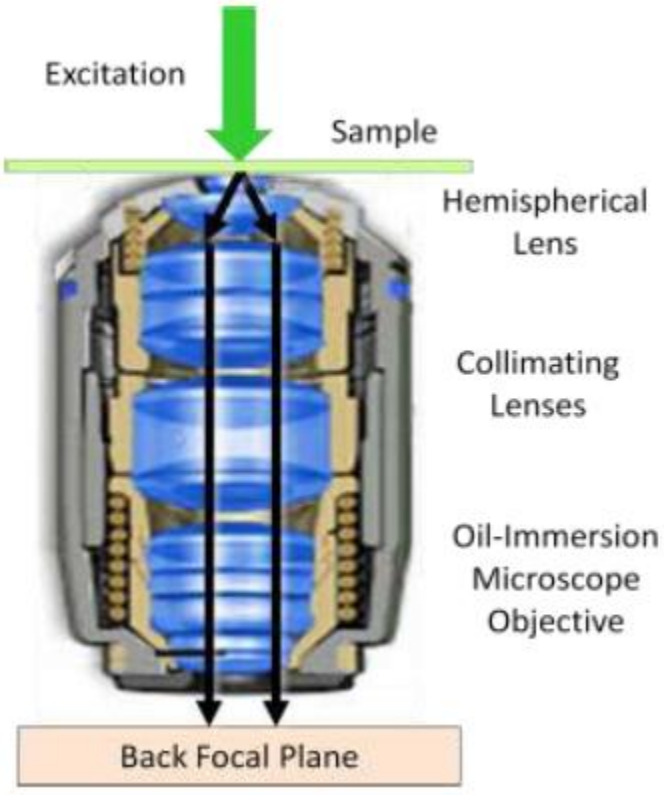

Figure 1.3 Schematic of sample-high NA microscope objective arrangement for collecting leakage radiation from the sample [3].

SPP tomography [5-8] permits the study of interference features formed at the metal-air interface of a sample due to the superposition of SPP beams with high fidelity[9-10]. In this work, SPP tomography is used to study the formation of a single SPP standing wave due to the superposition of two SPPs traveling in opposite directions in a DLSPPW. The resulting SPP standing wave has a formation of an interference pattern in the DLSPPW with well defined interference fringes. The presence of the dark fringes in the observed interference pattern indicates that the net energy flow inside of the waveguide was zero [11-12]. This is due to the fact that the light propagating in each opposite direction carried equal amount of energy.

Also presented in this paper is a quantum description of the formation of an electromagnetic standing wave with relatively intense light. In this experiment, the single photon events were not measured. Regardless, it is interesting to analyze the experimental results, focusing attention to the quantum nature of light. This analysis is reasonable because, according to Bohr's correspondence principle [13], classical optics should be an extreme instance of the more precise quantum description of light. Since a full quantum-electrodynamic description would be unnecessarily complicated [14-15], what will be presented is a quantum description based on the use of the most simple of the three common interpretations of the photon[16]. One is that a photon is what produces a "click" in a photodetector. Feynman's description of interference, which states that the probability of an event is given by $p = |\Phi|^2$, where Φ is a complex number which is the probability amplitude of the event, was also used [17]. These ideas were chosen because this approach allows one to explore the classical limit of the quantum theory without more complexities than are required by a quantum description. Nevertheless, this basic approach allowed us to obtain the classical limit of the analytical expression of the transversal wavefunction of the photons in an

electromagnetic standing wave. In addition, we found that in the classical limit, there is a simple relationship between the quantum mechanical probability wave and the electric and magnetic fields of the standing wave.

The interference observed in the standing SPP wave can be easily explained by using an argument based on the wave nature of light [11,18]. However, if we wish to use a corpuscular description of light, we run into difficulty when aspects of the interference phenomena are explained. This difficulty arises when one tries to explain how a corpuscle of light passes through a dark interference fringe without being detected. This is the photon propagation paradox [5-6,10]. This paradox can be explained by using a pure wave description of light according to Bohr's Complementarity Principle in its most orthodox form. This states that a photon can behave either as a particle or a wave, but never as both [19-20]. Modern interpretation of the principle does not take it in its most orthodox form and interprets it as "wave-particle duality". This interpretation allows for both the wave and particle nature of light to co-exist but it postulates that a stronger manifestation of the particle nature of light will lead to a weaker manifestation of the wave nature of light and vice versa[19,21-22].

This paper is organized as follows: In Chapter II the experimental set up used in this work is described along with the experimental results is presented. Chapter III is dedicated to a classical discussion of the experiments. A phenomenological quantum description of the formation of an electromagnetic standing wave, which is compatible with the experimental results, is presented in Chapter IV. Finally, the conclusions of this work are given in Chapter V.

CHAPTER II

SAMPLES AND EXPERIMENTAL ARRANGEMENT

The sample used consisted of a 25 µm long, single mode DLSPPW with a width of 600 nm. The waveguide was fabricated on a glass substrate. A 50 nm thick gold layer was initially deposited on top of a 1 nm thick chromium adhesion layer. The gold layer was topped with a 150 nm thick PolyMethylMethAcrylate (PMMA) layer. The wave guide was etched into the PMMA layer using e-beam lithography [4] as sketched in Figure 2.1.

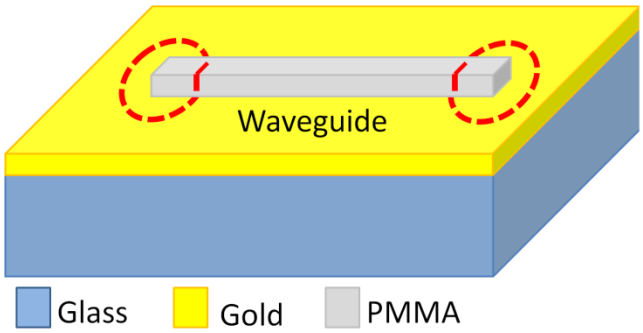

Figure 2.1: Sketch of fabricated DLSPPW. The discontinuous circles illustrate the position of the laser spots used to excite the SPPs by scattering at the extremes of the waveguide.

The excitation source for the SPPs was provided by a 10mW He-Ne laser (λ = 632.8 nm). The laser beam was split evenly by a cube beam splitter and then deflected by mirrors towards a low numerical aperture (NA=0.65, 40×) microscope objective lens at slightly different angles. The lens focused the beam onto spots with diameters of ~5 µm onto opposite edges of the waveguide as shown in Fig 2.1. The excited SPPs propagate towards each other inside the waveguide. The leaked radiation was collected

by an immersion oil objective lens (NA=1.49, 100×). Magnification, aberration correction, and image formation were done by a set of lenses that are internal to the microscope. The leakage radiation is further partially reflected by a beam splitter into a charge coupled device (CCD) camera which captures the image of the sample surface emission (SE). A second CCD camera collects the image formed in at the back focal place (BFP) of the objective lens. A BFP image corresponds to the Fourier Plain (FP) with respects to the sample surface emission and is therefore a two-dimensional map of the momentum distribution of the SPPs that are excited in the plane of the sample being observed. Several accessories, such as a beam block, linear polarizer, and a half wave plate, can be inserted after the high numerical aperture object lens. The light at the point is in the BFP. Since the light from the two excitation point are traveling in opposite directions, the leakage radiation from these points are separated allowing us to use certain accessories, such at the half wave plate, on one beam while leaving the other one unaffected. This provides much flexibility to the SPP tomography arrangement. The entire experimental setup is shown below in figure 2.2.

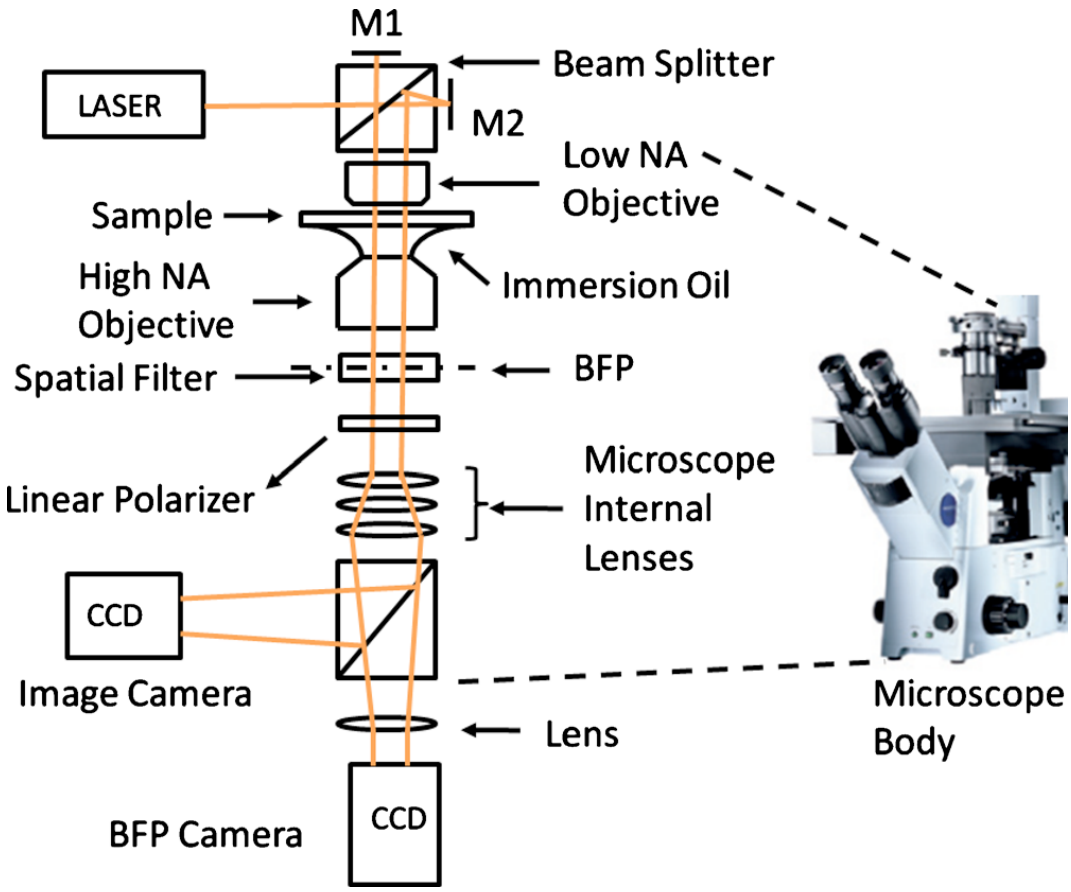

Figure 2.2 Schematic of the setup used to excite and collect leakage radiation from SPPs[4].

Experimental Results

A single SPP excitation in one DLSSPW is shown in Figure 2.3 with the SE and FP images repetitively. Fig 2.3(a) shows SPP propagation from the left to the right in the DLSPPW. A propagation length of ~12 µm was estimated from a line profile (not shown) along the SPP path. Figure 2.3 shows a central bright spot with is caused by the transmission of uncoupled light through the sample. The FP image shows a straight vertical segment at the right extreme of the image. This is the signature of a SPP traveling from left to right in a single mode DLSPPW[5-8,9-10]. The FP image also shows other arcs that correspond to SPPs that are excited at the gold-air interface of the sample. The ratio of the distances of the traces to the central spot is equal to the ratio

of the corresponding effective refractive indexes(n_{eff}) of the excited SPPs. Using the reported value of ~1.03 for n_{eff} for the SPP excited in the gold air interface[9], n_{eff} ~1.1 was determined for the DLSPPW mode. The wavelength of an SPP excited in a waveguide is $\lambda_{SPP}=\lambda/n_{eff.}$ This yields a wavelength for the SPP to be 577 nm.

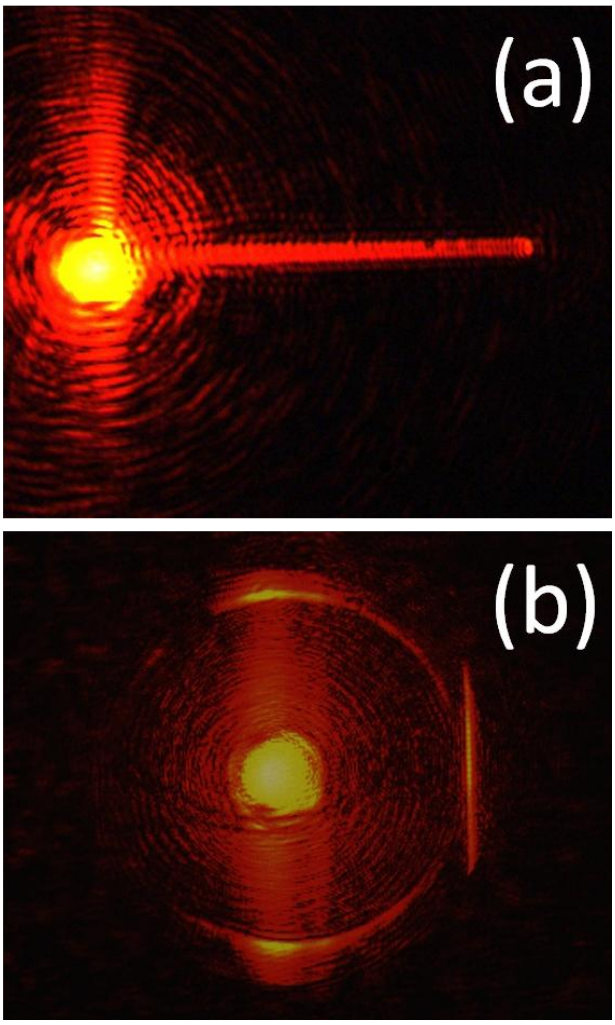

Figure 2.3: (a) SE and (b) FP images corresponding to a single SPP excited in the DLSPPW.

Two beams were used to excite SPPs simultaneously at opposite ends of the DLSPPW. The SE images corresponding to the scenario are shown in Fig 2.4. The existence of two SPP beams traveling in opposite directions was confirmed by the

presence of two vertical straight line segments at the right and left extremes of the corresponding FP images (not shown). The leakage radiations associated with each of the two SPPs have the same polarization state because the excited SPPs travel in opposite directions [23]. This was confirmed because the SE image shown in Fig 2.4 was taken using a linear polarizer that was inserted in the optical path of the leakage radiation with its transmission axis aligned with the polarization of the leaked lights. In addition to the linear polarizer, a beam blocked was used to block the direct laser light that can be observed in Fig 2.3. The interference fringes as seen in Fig 2.3(a) have a separation of ~ 286 nm. The fringes observed correspond to the formation of a stationary wave in the waveguide. Because of propagation losses coming from both beams, the intensity of the two beams are closely matched at the center of the waveguide yielding better defined fringes at the center. The distance between consecutive bright fringes is equal to the half the wavelength of the wave that is propagating in the DLSPPW. Using this, a value form the wavelength of the SPP was found to be ~ 572 nm which is in excellent agreement with the value found from the FP image shown in Fig2.3(b).

The interference pattern can be eliminated using a quantum eraser arrangement [9,24]. This arrangement was achieved by introducing a linear polarizer and a half-wave plate in the BFP of the high NA objective along the optical path of the leakage radiation that is associated with only one of the SPPs. The half wave plate was rotated so that the polarization orientation of the leakage radiation associated with that specific SPP was changed to become polarized orthogonal to the unaffected SPP. Doing so resulted in the elimination of the interference fringes as observed in Fig2.4(b).

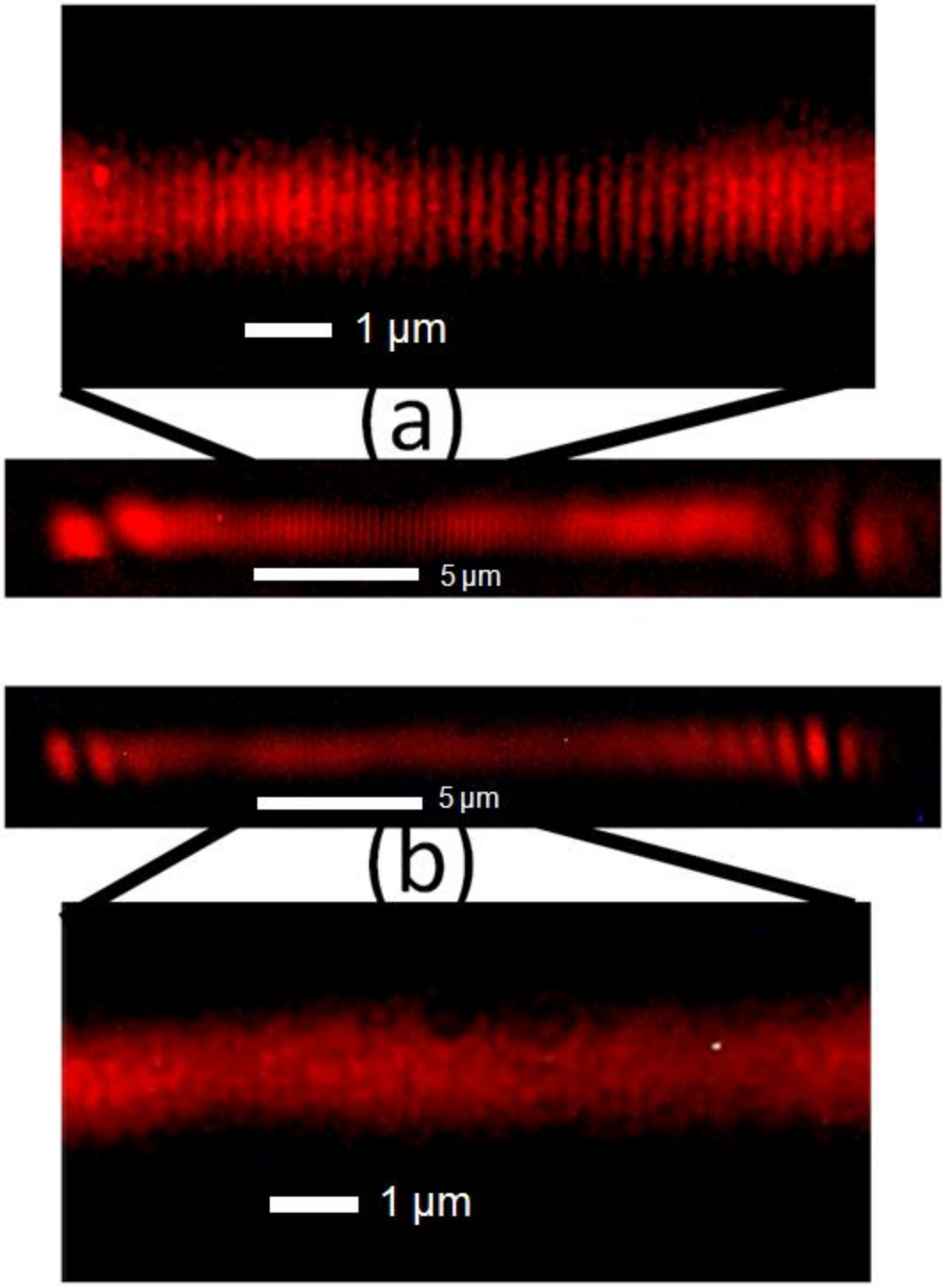

Figure 2.4: SE images corresponding to two SPPs excited simultaneously in the DLSPPW. The images were obtained inserting after the high NA objective lens (a-b) a linear polarizer (b) followed by a half wave plate.

CHAPTER III

CLASSICAL DISCUSSION OF THE EXPERIMENTAL RESULTS

The stationary wave that was formed in the DLSPPW can be understood by assuming in the first approximation that any losses due to the leakage radiation is small. We also took that the electric field distribution near the center of the waveguide is similar to the electric field distribution caused by the superposition of two plane waves that are propagating in the opposite directions. This topic has been previously discussed in several optics textbooks [11,18]. In this approximation, both the electric and magnetic field distribution in the interference patter corresponding to the stationary wave are described by the following[19]:

$$E_T(x,t) = 2E_o \sin(kx)\cos(\omega t) \tag{3.1}$$

$$B_T(x,t) = -2B_o \cos(kx)\sin(\omega t) \tag{3.2}$$

Where $k=2\pi/\lambda_{SPP}$, and $\omega=2\pi c/\lambda$ where c is the speed of light. E_o and B_o are the amplitudes of the electric and magnetic field of both waves respectively. Figure 3.1 shows a series of plots of the instantaneous values of E_T (red) and B_T (blue) in an area of $2\lambda\times2\lambda$ over a period of time. In agreement with equations 3.1 and 3.2, the nodes of E_T occur at the antinodes of BT and vice versa. Figure 2.5(a,d) shows that when $B_T=0$, we have a maximum value for $|E_T|$ and vice versa. This is consistent with the energy conservation principle. We find that all the wave energy is carried by the magnetic field, when the electric field is zero everywhere and vice versa[18-19]. And when neither B_T nor E_T are zero, the energy is distributed between both of the fields. This description of the interference corresponds to a pure wave description of light. However, as discussed previously, light should exhibit particle properties at all times[19,21-22,25]. Even though it is not customary, using a particle interpretation of light we should be able to explain how photons could pass through the interference minima which were formed in the center of the DLSPPW as seen in figure 2.4(a). Figure 2.5 illustrates how localized

photon traveling at the speed of light could pass through the interference pattern. The white disks represent the photons as they transverse the DLSPPW. It was assumed that photons can exist wherever there is electromagnetic energy. This is in correspondence with the latest theoretical ideas about the photon wavefunction which establishes that the probability of a photon to be detected at a particular position in the pattern is proportional to $\alpha_1|E_T|^2 + \alpha_2|B_T|^2$, where $\alpha_{1,2}$, are appropriate dimensional constants[16]. Fig 3.1(a,f) show that photons should be at the antinodes of the magnetic field when the electric field is zero everywhere and vice versa.

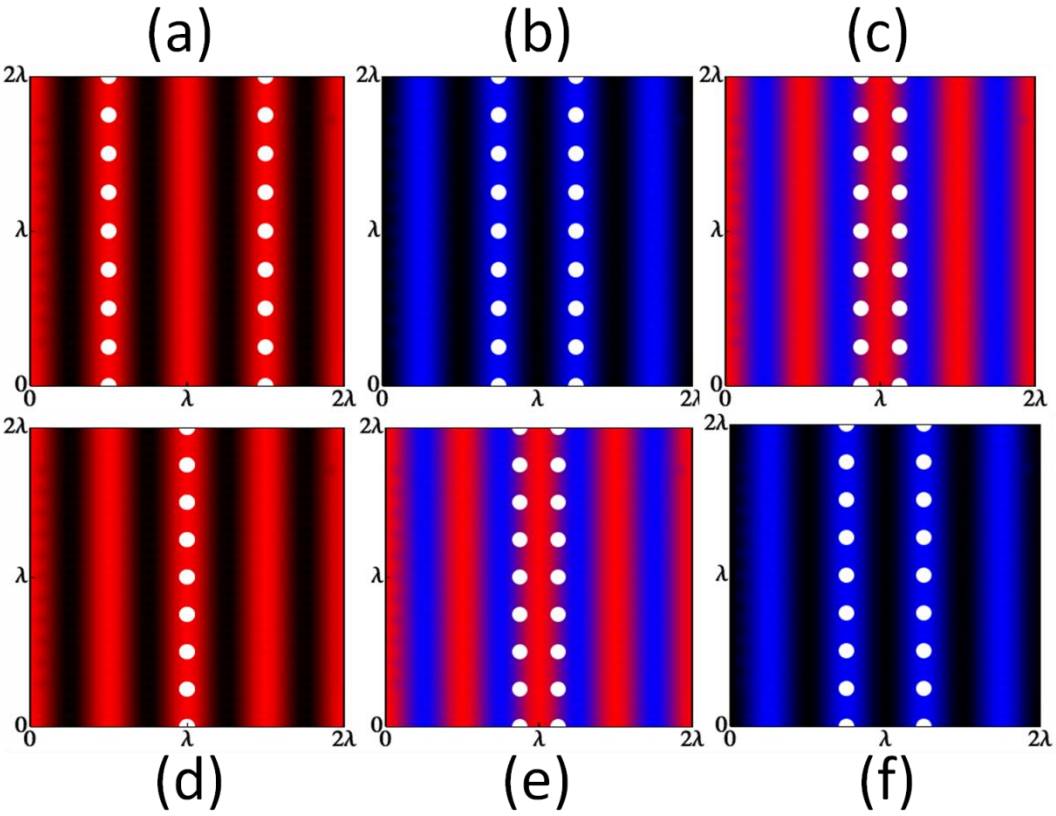

Figure 3.1: Calculated values of the instantaneous magnitude of the electric (red) and magnetic (blue) fields in the region occupied by the SPP standing wave. The time increases from (a) to (f). The small white disks represent spatially localized photons traveling at the speed of the light.

This brings the questions of why are photons not detected at the nodes of the electric field. The reason is well known: common photodetectors are only responsive to the electric field[11,18]. Despite this, Fig 2.4(b) demonstrates that photons passing through the nodes of the electric field in a standing wave can be detected by SPP tomography in a quantum eraser arrangement[5-6]. In general, we assume that the SE images are a map of the points on the gold layer in which there is leaking light and that FP images are maps of the directions in which the leakage occurs[5-6]. Fig 2.4(a) gives a useful exception to this rule[13]. Here we find that the dark fringes in Fig 2.4(a) do not mean that there is no light leaked from the corresponding point in the gold layer. In contrast, the absence of the dark fringes in fig 2.4(b) indicates that the light leaks from the gold layer in the regions where the nodes of the standing wave were formed. The origin of the interference pattern as shown on the SE image comes from the superposition at the CCD camera of the light leaked in opposite directions from the nodes of the standing wave. The erasure of the interference fringes in the SE image due to the introduction and rotation of the half wave plate cannot change the origin of the leakage radiation from the gold layer since the plate was inserted after the light was leaked. Therefore, the SE image shown in Fig 2.4(b) is a reliable map of the points of the sample surface where the leakage radiation comes from. This method permits us to detect photons while passing through the nodes of the standing wave formed in the DLSPPW. In contrast with the SE image shown in Fig2.4(b), the SE image shown in fig 2.4(a) is an incorrect map of the point of the sample surface that leaked but permits one to observe at the far field the stationary wave formed in the waveguide.

Expressions 3.1 and 3.2 may be rewritten in the following forms:

$$E_T(z,t) = \mathrm{Re}\left[2E_o \sin(kz) e^{i\omega t} \right] \tag{3.3}$$

$$B_T(z,t) = \mathrm{Im}\left[-2B_o \cos(kz) e^{i\omega t} \right] \tag{3.4}$$

Where Re and Im are the real and imaginary parts respectively. Using equations 3.1, the intensity of the standing wave in the center of the DLSSPW can be approximated with the following expression[12,18]:

$$I(z)=\tfrac{1}{2}c\varepsilon E^2(z)=4I_o\sin^2\left(kz\right) \tag{3.5}$$

Where ε is the effective electrical permittivity of the propagation medium and I_o is the intensity of each of the waves whose superposition resulted in the standing waves, i.e[12,18]:

$$I_o=2\alpha_E^2E_o^2\ ,\ \alpha_E=\sqrt{\tfrac{1}{4}c\varepsilon} \tag{3.6}$$

I(z) corresponds to the interference patter shown in figure 2.4(a). Intensity minima I(z)=0, and intensity maxima, $I(z)=4I_o$ occur at the dark and bright fringes of the pattern respectively. In optics is customary to introduce the so called optical disturbance, $U_E(z)$, in the following way[26]:

$$E_T(z,t)=\mathrm{Re}[U_E\left(z\right)e^{i\omega t}] \tag{3.7}$$

Comparing 3.7 to 3.3 results in:

$$U_E(z)=2E_o\sin\left(kz\right)=E(z) \tag{3.8}$$

Therefore, using (3.5) and (3.7-3.8) permits one to express the intensity of the standing wave in terms of the optical disturbance in the following way:

$$I(z)=2\alpha_E^2\left|U_E(z)\right|^2 \tag{3.9}$$

It is worth noting that $I(z)$ is the intensity that would be measured by a common photodetector which is only responsive to the electric field. Recent advances in active magnetic optical metamaterials permits a possible future realization of advanced optical photodetectors that are equally responsive to both electric and magnetic fields. Such advanced photodetectors would measure the presence of light wherever the electric or magnetic field of the standing wave is not simultaneously zero [27-29]. Therefore, if an

advanced photodetector (which equally responsive to both electric and magnetic fields) were used to measure the intensity of an electromagnetic standing wave, it would measure the constant intensity, I_a, given by the following expression[12,18]:

$$I_a = \alpha_E^2 E_T^2(z) + \alpha_B^2 B_T^2(z) = 2I_o \ , \ \alpha_B = \sqrt{\frac{1}{4}\frac{c}{\mu}} \tag{3.10}$$

where μ is the effective magnetic permeability of the propagation medium. Therefore such an advanced photodetector would not register the formation of a standing wave interference pattern. This is in excellent correspondence with the uniform intensity distribution along the waveguide seen in Fig. 2.4(b). In the Optics of active magnetic optical metamaterials, it is convenient to introduce a generalized optical disturbance given by the following expression:

$$U_g(z) = \alpha_E U_E(z) + i\,\alpha_B U_B(z) \tag{3.11}$$

Where $U_E(z)$ is related with the electric field as above, and the magnetic optical disturbance, $U_B(z)$, is related with the magnetic field in the following way:

$$B_T(z,t) = \mathrm{Im}[U_B(z)e^{i\omega t}] \tag{3.12}$$

Comparing (3.12) and (3.4) results:

$$U_B(z) = -2B_o \cos(kz) \tag{3.13}$$

Using (3.10-3.11) with (3.8) and (3.13) permits one to express I_a in terms of the generalized optical disturbance in the following way:

$$I_a = \left|U_g(z)\right|^2 \tag{3.14}$$

CHAPTER IV

PHENOMENOLOGICAL QUANTUM DESCRIPTION OF THE FORMATION OF AN ELECTROMAGNETIC STANDING WAVE

A quantum description of the interfereance pattern is required when the illumination source used uses feeble light or single photons. In these experiments performed, the interference pattern is formed gradually by the accumulation of numerous "click", i.e., individual photon-detection[30]. If the experiment performed above were repeated but using feeble light instead, it should be expected that the same results would be obtained after a large number of single-photon events are recorded. Using a quantum picture, the intensity where the standing wave is formed along the DLSPPW may be approximated by the following expression[31-32]:

$$I(z) = Nh\nu \,|\, \Omega(z) \,|^2 \tag{4.1}$$

Where, h is Planck's constant, ν=c/λ, N is the average number of photons that pass per unit time through the transversal section of the waveguide and, following Feynman's approach for describing interference [32], $\Omega(z=z_o)$ is the probability amplitude per unit area (probability amplitude density) of detecting a photon passing through the transversal section of the waveguide at $z=z_o$ near the center of the waveguide. Due to Bohr's correspondence principle, classical and quantum descriptions should give equal results when a large enough number of photons are coupled to the DLSPPW. Because of this, $I(z)$ in (3.9,4.1) should be equal resulting in the following proportionality relation between $\Omega(z)$ and $U_E(z)$[32]:

$$\left|\Omega_E(z)\right| = \beta U_E(z) \;\; , \; \beta = \sqrt{\frac{2}{Nh\nu}}\alpha_E \tag{4.2}$$

In the classical limit, relation (4.2) states that the probability amplitude per unit area of registering a "click" at the point $z=z_o$ is directly proportional to the optical disturbance

value at that point. This provides a way to calculate the probability distribution of "clicks" along the DLSPPW without having to rely on the mathematical subtleness of more elaborated quantum theories of photons[14-16]. Because of this, satisfying relation (4.2) can be seen as a mandatory test for any successful quantum theory of photons. Expression (4.1) provides a phenomenological definition of Ω. Therefore, calculated values of Ω_E using any quantum theory of photons (in the classical limit) and the values of Ω_E calculated using expression (4.2) should match. The sub index *E* of Ω was introduced in (4.2) for emphasizing that Ω_E refers to the photodetection events using a common photodetector that is only responsive to the electric field. However, since photons can be detected wherever there is electromagnetic energy in the standing wave, a more general expression for Ω can be obtained comparing (3.14) and (4.1). This results in the following expression:

$$\left|\Omega_g(z)\right| = \sqrt{\frac{1}{Nh\nu}}\left|U_g(z)\right| \tag{4.3}$$

Expression (4.3) states that, in the classical limit, the most general expression of the probability amplitude density of registering a "click" at $z=z_o$ (using an advanced optical photodetector that is equally responsive to both electric and magnetic fields) is directly proportional to the value of the generalized optical disturbance at that point. Using a quantum description, the uniform intensity distribution along the waveguide seen in Fig. 2.4(b) can be explained by the unchanging probability per unit area, *p*, of finding a photon along the DLSPPW. In the classical limit, and by using expressions (3.10,3.14,4.3) and (3.8,3.11,3.13), *p* can be expressed in terms of the transversal wavefunction ψ(*z*,*t*) [23,29-30] of the photons in an electromagnetic standing wave in the following way:

$$\left|\Psi(z,t)\right|^2 = \left|\Omega_g\left(z\right)\right|^2 = \frac{2I_o}{Nh\nu} \tag{4.4}$$

Where:

$$\Psi(z,t)=\left|\Omega_g\left(z\right)\right|e^{i\omega t}=\sqrt{\frac{\alpha_E^2E^2(z)+\alpha_B^2B^2(z)}{Nh\nu}}\,e^{i\omega t} \tag{4.5}$$

The complex exponential factor was included in (4.5) because $\psi(z,t)$ describes a stationary state [17]. The classical limit of the transversal wavefunction, $\psi(z,t)$, does not have nodes at the regions that are occupied by the dark fringes of the standing wave interference pattern as shown in Fig. 2.4(a) because the magnetic field have antinodes there. The electric field does have nodes at the dark fringes but the amplitude of the transversal photon wavefunction is not exclusively determined by the electric field of the standing wave. It is worth noting that for a plane wave $E(z)=E_o$, $B(z)=B_o$, $E_o=cB_o$ [19,26]; therefore, for a plane wave $|\Omega_g|$ is given by the following expression:

$$\left|\Omega_{g,pw}\left(z\right)\right|=\left|\Omega_{E,pw}\left(z\right)\right|=\sqrt{\frac{2}{Nh\nu}}\alpha_E\,E_o \tag{4.6}$$

In the classical limit, the amplitude of the transversal wavefunction of the photons in a electromagnetic plane wave, $\psi_{pw}(z,t)$, is proportional to the amplitude of the electric field:

$$\Psi_{pw}(z,t)=\sqrt{\frac{2}{Nh\nu}}\alpha_E\,E_o e^{i(kz-\omega t)} \tag{4.7}$$

In the experiments described in Chapter II, individual photons were not detected. However, as Feynman emphasized “light is made of particles” [33]. Also, the corpuscular nature of SPP excitation has been demonstrated experimentally [34-35]. Because of this, we can predict that if the experiments described in Chapter II were repeated but using feeble light, then SPP tomography will permit the detection of single photons while they are passing through the “will be” dark fringes of the standing wave interference pattern. If the experiments were run using an advanced photodetector (one which is equally responsive to both electric and magnetic fields) then a uniform illumination along the waveguide similar to the shown in Fig. 2.4(b) would be measured. Therefore, an

electromagnetic standing wave provides a simple but effective method for producing a spatially localized pure magnetic field oscillating at very high frequencies. This can be useful for things such as for testing novel active magnetic optical metamaterials[27].

CHAPTER V

CONCLUSION

We have presented classical and a phenomenological quantum descriptions of experiments where SPP tomography was used to study the formation of SPP standing waves. We showed that SPP tomography in a quantum eraser arrangement has the capability of observing light passing through the dark fringes of the observed standing wave interference pattern. We were able to obtain the classical limit of the analytical expression of the transversal wavefunction of the photons in an electromagnetic standing wave. We also obtained that in the simple relationship between the quantum mechanical probability wave, $\psi(z,t)$, and the electric and magnetic fields of the standing wave in the classical limit. We claim that the experimental results presented in this work support the more modern ideas about the wave-particle duality of photons and of the photon wavefunction.

REFERENCES

1. H. Raether, *Surface Plasmons on Smooth and Rough Surfaces and on Gratings* (Springer-Verlag, Berlin 1988)
2. Akimov, A. Mukherjee, C. L. Yu, D. E. Chang, A. S. Zibrov, P. R. Hemmer, H. Park, M. D. Lukin, Nature **450**, 402 (2007).
3. L. Grave de Peralta, Lecture Notes, Physics 5300, Spring 2011, Department of Physics, Texas Tech University.
4. A. Krishnan, C. J. Regan, L. Grave de Peralta, and A.A. Bernussi, Applied Phys. Letters, **97**, 231110 (2010).
5. L. Grave de Peralta, R. Lopez-Boada, A. Ruiz-Columbie, S. Park, and A. A. Bernussi, J. of Appl. Phys. **109**, 023101 (2011).
6. A. Houk, R. Lopez-Boada, A. Ruiz-Columbie, S. Park, and A. A. Bernussi, and L. Grave de Peralta, Erratum, J. of Appl. **109**, 119901 (2011).
7. C. J. Regan, A. Krishnan, R. Lopez-Boada, L. Grave de Peralta, and A.A. Bernussi, Appl. Phys. Lett. **98**, 151113 (2011).
8. S. P. Frisbie, C. Chesnutt, M. E. Holtz, A. Krishnan, L. Grave de Peralta, and A. A. Bernussi, IEEE Photonics Journal, **1**, 153 (2009).
9. J. Ajimo, M. Marchante, A. Krishnan, A.A. Bernussi, and L. Grave de Peralta, J. of Appl. Phys. **108**, 063110 (2010).
10. L. Grave de Peralta, "Study of interference between surface plasmon polaritons by leakage radiation microscopy," J. Opt. Soc. Am. B **27**, 1513 (2010).
11. M. Born and E. Wolf, *Principles of Optics*, (Pergamon Press, New York, 1964).
12. F.L. Pedrotti, L.S Pedrotti and L.S Pedrotti, *Introduction to Optics* (Pearson Prentice Hall, New Jersey, 2007).
13. B. L. Van Der Waerden, *Sources of Quantum Mechanics* (G. Holton, Editor, Dover, New York, 1967).
14. M. O. Scully and M. S. Zubairy, *Quantum Optics* (Cambridge University Press, Cambridge, 1997).
15. 14. R. P Feynman and A. R. Hibbs, *Quantum Mechanics and Path Integrals* (MacGraw-Hill, New York, 1965).
16. B. J. Smith, and M. G. Raymer, New Journal of Physics **9**, 414 (2007).
17. R. P. Feynman, R. B. Leighton and M. Sands, *The Feynman Lectures on Physics* (Vol II, Addison-Wesley, Massachusetts, 1965).
18. E. Hetcht, *Optics* (Fourth Edition, Pearson-Addison Wesley, 2002).
19. S. Bandyopadhyay, Physics Letters A, **276**, 233 (2000).
20. N. Bohr, "The Quantum Postulate and the Recent Development of Atomic Theory," Nature (Supplement), **121**, 580 (1928).
21. B-G Englert, "Fringe Visibility and Which-Way Information: An Inequality," Phys. Rev. Lett., **77**, 2154 (1996).

22. E.J. Galvez and M. Beck, *Education and Training in Optics 2007*, M. Nantel Ed. (2007). Online posting: http://spie.org/etop/etop2007.html.
23. S.P. Frisbie, C. Chesnutt, J. Ajimo, A.A. Bernussi, and L. Grave de Peralta,Opt. Commun. **283**, 5255 (2010).
24. W. Holladay, *Physics Letters A*, **183**, 280 (1993).
25. S. S. Afshar, E. Flores, K. F. McDonald, and E. Knoesel, Foundations of Physics, **37**, 295 (2007).
26. J. W. Goodman, *Introduction to Fourier Optics* (McGraw-Hill, New York, 1968).
27. K. Münter, R. Pape, M. Spitzer, J. Glimm, and R. Bitzer, in *Proceeding of the 15th International Zurich Symposium & Technical Exhibition on Electromagnetic Compatibility* (EMC Zurich 2003).
28. M. Burnessi, T. Kampfrath, D. van Oosten, J. C. Prangsma, B. S. Song, S. Noda, and L. Kuipers, Phys, Rev. Lett. **105**, 123901 (2010).
29. S. Vignolini, F. Intonti, F. Riboli, L. Balet, L. H. Li, M. Francardi, A. Gerardino, A. Fiore, D. S. Wiersma, and M. Gurioli, Phys. Rev. Lett. **105**, 123902 (2010).
30. A. Zeilinger, G. Weihs, T. Jennewein, and M. Asppeimeyer, Nature **433**, 230 (2005).
31. D. Bohm, *Quantum Theory*, Englewood Cliffs, N. J., Prentice Hall, 1951.
32. L. Grave de Peralta, J. of Appl. Phys. **108**, 103110 (2010).
33. R. P. Feynman, *QED: The strange theory of light and matter* (Princeton University Press, 1985).
34. E. Altewischer, M. P. van Exter, and J. P. Woerdman, Nature **418**, 304 (2002).
35. A. V. Akimov, A. Mukherjee, C. L. Yu, D. E. Chang, A. S. Zibrov, P. R. Hemmer, H. Park, M. D. Lukin, Nature **450**, 402 (2007).